Volume 11
Number 6
14 February 2023
Pages 1163–1380

Journal of Materials Chemistry B

Materials for biology and medicine

rsc.li/materials-b

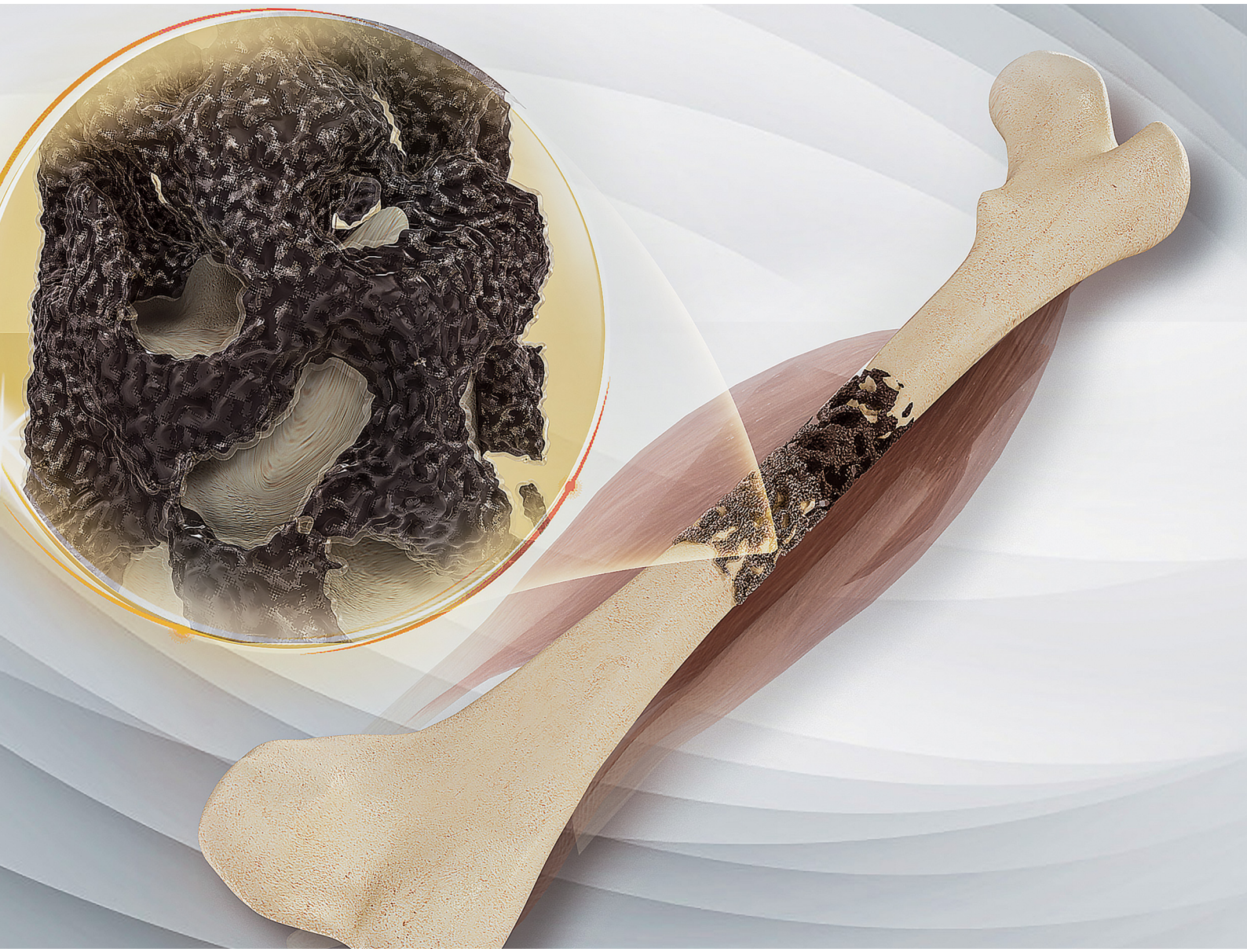

ISSN 2050-750X

ROYAL SOCIETY OF CHEMISTRY

PAPER
Dong Qiu, Hua Tian *et al.*
A pH-neutral bioactive glass coated 3D-printed porous Ti6Al4V scaffold with enhanced osseointegration

10 YEARS ANNIVERSARY

Journal of Materials Chemistry B

ROYAL SOCIETY OF CHEMISTRY

PAPER

View Article Online
View Journal | View Issue

Cite this: J. Mater. Chem. B, 2023, 11, 1203

A pH-neutral bioactive glass coated 3D-printed porous Ti6Al4V scaffold with enhanced osseointegration†

Xinguang Wang,‡[ab] Qirui Guo,‡[cd] Yizhen He,[ab] Xiao Geng,[ab] Cheng Wang,[ab] Yang Li,[ab] Zijian Li,[ab] Caimei Wang,[e] Dong Qiu *[cd] and Hua Tian *[ab]

Osseointegration is vital for the success of non-degradable implants like those made of titanium alloys. In order to promote osseointegration, implants are made porous, providing space for bone ingrowth. Despite extensive optimization of the pore geometry and porosity, bone ingrowth into implants is still marginal; further modification to promote bone ingrowth as well as osseointegration becomes paramount. In this study, a pH neutral bioactive glass with the composition of 10.8% P_2O_5–54.2% SiO_2–35% CaO (mol%; hereinafter referred to as PSC) was successfully coated on 3D-printed porous Ti6Al4V scaffolds using an *in situ* sol–gel method. This PSC coating is strongly bonded to the substrate and quickly induces the formation of hydroxyapatite on the scaffold surface upon contact with body fluid. *In vitro*, the PSC-coated Ti6Al4V scaffolds showed superior biocompatibility, cell proliferation promotion, cell adhesion, osteogenic differentiation and mineralization compared to their bare counterparts, implying better osseointegration. *In vivo* experiments confirmed this expectation; after being implanted, the coated scaffolds had more bone ingrowth and osseointegration, and consequently, higher push-out strength was achieved, proving the validity of the proposed concept in this study. In conclusion, PSC coating on 3D-printed porous Ti6Al4V scaffolds can improve osteogenesis, bone ingrowth, and osseointegration. Together with the versatility of this *in situ* sol–gel coating method, titanium alloy implants with better biological performances may be developed for immediate clinical applications.

Received 6th October 2022,
Accepted 28th November 2022

DOI: 10.1039/d2tb02129c

rsc.li/materials-b

1. Introduction

With the development of 3D printing technology, 3D-printed titanium alloy (Ti6Al4V) porous implants have been widely used in orthopedics and stomatology, with good clinical outcomes.[1,2] Compared with traditional non-porous implants, 3D-printed Ti6Al4V porous implants can reduce the elastic modulus and stress shielding by adjusting the pore size, geometry and porosity, and can promote the growth of trabecular bone into the pores, realizing better osseointegration between the bone and the implant.[3–5] However, the inherent bio-inertness of titanium alloys restricts the degree of bone ingrowth, thus osseointegration is still rather limited and the risk of prosthesis loosening remains fairly high.[6,7] Undoubtedly, this is adverse to implant survival time and the clinical effect of surgery.[8,9] Therefore, the surface modification of 3D-printed Ti6Al4V implants has recently become an emerging focus.[10] Biogenic growth factors, such as bone morphogenetic protein-2,[11] type-I collagen,[12] and functional hydrogel coating,[13] have been introduced to promote bone ingrowth and osseointegration; however, they have certain disadvantages such as high cost, complicated manufacturing process, unstable quality, and difficult to preserve nature.[8] Mineral coating, for example Ca/P by microarc oxidation,[14] was also developed on 3D-printed Ti6Al4V porous implants with lower cost and stable quality, while its promotion of bone ingrowth was far from satisfactory, significantly hampering their clinical applications.[15]

In recent years, bioactive glasses (BGs) have received increasing attention[16–18] because they show the best performance on osteogenesis and angiogenesis in the absence of biogenic growth factors,[19] the two essential elements for ideal bone regeneration materials.[20,21] Since Larry Hench created a kind of BG named 45S5, it has been developed and applied in

[a] Department of Orthopedics, Peking University Third Hospital, Beijing, 100191, China. E-mail: tianhua@bjmu.edu.cn
[b] Engineering Research Center of Bone and Joint Precision Medicine, Ministry of Education, Beijing, 100191, China
[c] Beijing National Laboratory for Molecular Sciences, CAS Research/Education Center for Excellence in Molecular Sciences, Institute of Chemistry, Chinese Academy of Sciences, Beijing, 100190, China. E-mail: dqiu@iccas.ac.cn
[d] University of Chinese Academy of Sciences, Beijing, 100049, China
[e] Beijing 3D Printing Orthopedic Application Engineering Technology Research Center, Beijing, 102200, China

† Electronic supplementary information (ESI) available. See DOI: https://doi.org/10.1039/d2tb02129c

‡ Xinguang Wang and Qirui Guo contributed equally to this work.

clinical practice.[22] 45S5 is as effective as an iliac crest graft to maintain correction and achieve fusion in adolescent idiopathic scoliosis.[23] Besides, studies have also shown that 45S5 coating can be realized on the surface of 3D-printed microporous titanium alloy scaffolds, which has good biocompatibility and can promote the attachment, proliferation and differentiation of human bone marrow stromal cells (BMSCs).[24] However, 45S5 was prepared using the melt-quenching method, and the high pH of the dissolved product, low degradation rate, crystallization during sintering, and small specific surface area of the product lead to its relatively low biological activity.[25]

The newly developed pH-neutral BG with the composition of 10.8% P_2O_5–54.2% SiO_2–35% CaO (mol%; hereinafter referred to as PSC)[26,27] is especially promising because it has circumvented two most striking drawbacks of classical BGs, namely, the high pH and low degradation rate.[25,28] PSC can provide a relatively neutral pH (about 7.8) and release large amounts of phosphate ions and silicate ions when immersed in body fluids, which were beneficial to new bone growth.[25] Compared to 45S5 and beta-tricalcium phosphate (β-TCP), PSC showed better promotion of the osteogenic and angiogenic differentiation of BMSCs.[28] However, direct coating of PSC on scaffolds is not straightforward because PSC powders are hard to be sprayed and firmly attached to the surface. Instead, as PSC is made from a sol–gel process, a coating may be prepared by spaying the sol onto the surface. Unfortunately, the standard sol–gel process for PSC is very time-consuming (the gelling usually takes more than two weeks), thus the timely formation of coating is unrealistic.[25]

In this study, a fast sol–gel process for PSC preparation is developed, where the gelling time is reduced to a few minutes, thus enabling *in situ* formation of PSC coating. In detail, PSC was successfully coated onto the surface of 3D-printed porous Ti6Al4V scaffolds, and its effects on proliferation, adhesion, and mineralization of rat BMSCs and *in vivo* performances of osteogenesis, bone ingrowth, and osseointegration in a rabbit femoral defect model were evaluated.

2. Materials and methods

2.1 Design and manufacture of 3D-printed Ti6Al4V porous scaffolds

We designed 2 types of 3D-printed Ti6Al4V scaffolds: discs with a diameter of 7 mm and a thickness of 2 mm for material characterization experiments and cell experiments and cylinders with a diameter of 5 mm and a height of 6 mm for animal experiments (ESI† Fig. S1). The 3D-printed Ti6Al4V scaffolds in material characterization and animal experiments were porous with a pore size of 640 mm and a diameter of 400 mm, and the micropores are distributed in a diamond cubic lattice structure. This parameter has proved beneficial to bone ingrowth in previous studies.[4]

The manufacturing process of the 3D-printed Ti6Al4V porous scaffolds is as follows. The model of the 3D-printed scaffolds was imported into an electron beam melting rapid prototyping machine (Arcam AB, Molndal, Sweden) in a standard triangulation language format for layer-by-layer 3D printing using Ti6Al4V powders as the printing material. Subsequently, the scaffolds were ultrasonically cleaned in acetone, ethanol, and deionized water for 30 min.

2.2 Preparation of PSC-coated 3D-printed porous Ti6Al4V scaffolds

Synthesis of PSC. Preparation of calcium methoxyethoxide: 5 g of calcium metal grains (Sigma-Aldrich, St. Louis, MO, USA) were added into 120 mL of 2-methoxyethanol (Sigma-Aldrich, St. Louis, MO, USA), and reacted for 24 h at 80 °C under the protection of argon. The obtained mixture was centrifuged for 5 min at 8000 rpm, producing a clear calcium methoxyethoxide solution. 5 mL of calcium methoxyethoxide solution was heated to 1050 °C and dwelt for 2 h to measure its solid content.

Preparation of PSC: 50% phytic acid (PA) (Sigma-Aldrich, St. Louis, MO, USA) aqueous solution was dried and dissolved in ethanol for further use. Based on the composition of PSC (10.8% P_2O_5: 54.2% SiO_2: 35% CaO, mol%), tetraethylorthosilicate and PA were added into the as-formed phytic acid/ethanol solution. After 2 h of mixing under magnetic stirring, the as-prepared calcium methoxyethoxide solution was added to the mixture and further stirred for another 0.5 h. A clear and brownish-yellow PSC sol was obtained.

Fabrication of PSC coating on 3D-printed porous Ti6Al4V scaffolds. 3D-Printed porous Ti6Al4V scaffolds were submerged in 10 mol L^{-1} NaOH solution (Xilong Scientific, Guangdong, China) for 1 h at 80 °C and underwent subsequent ultrasonic cleaning in ionized water. The scaffolds were dried, dipped in the PSC sol for one minute and taken out. The sol quickly gelled within a few minutes. These scaffolds were calcined in the muffle furnace at 600 °C for 2 h, to generate the PSC-coated 3D-printed Ti6Al4V porous scaffolds.

2.3 Characterization of PSC bulk and PSC coating

Mechanical tests of the scaffolds. The compression tests of two groups of scaffolds (3D-printed porous Ti6Al4V scaffolds, hereinafter referred to as the Ti group; and PSC-coated 3D-printed porous Ti6Al4V scaffolds, hereinafter referred to as Ti-PSC groups) were carried out using a mechanical testing machine (Instron Co., USA) with a crosshead speed of 0.18 mm min^{-1}. The stress–strain curve was recorded and the elastic modulus, stiffness, yield strength, and compression strength were calculated. For each group of scaffolds, six samples with a diameter of 5 mm and a height of 6 mm were tested to ensure repeatability.

pH of PSC dissolutions. PSC was added to the simulated body fluid (SBF) (Hongyue Innovation Technology Co. Ltd, Beijing, China) at 1.5 mg mL^{-1}. The pH value of the system was measured using a pH meter (PB-10, Sartorius, Germany) for 60 h.

Bioactivity test of PSC. PSC was put into SBF at 1.5 mg mL^{-1} for 12, 24, and 36 h. The surface morphologies of PSC before and after the reaction with SBF were observed using a scanning electron microscope (SEM, JOEL-6700, Japan). The crystallographic structures of PSC before and after the reaction with SBF

were investigated *via* X-ray diffraction (XRD) (Rigaku, D/MAX2500) with Cu Kα radiation (λ = 1.54 Å) at a scanning rate of 4° min^{-1}. The data were collected for a 2θ range from 10° to 70°.

Fourier transform infrared spectroscopy (FTIR) (Bruker Equinox 55, Nexus, USA) was performed on PSC before and after the reaction with SBF. The scanning step size is 4 cm^{-1}, and the range is 4000–400 cm^{-1}.

Surface characterization of scaffolds. The microstructure of scaffolds was observed *via* SEM (JOEL-6700, Japan) coupled with energy-dispersive X-ray spectrometry (EDS).

Adhesion strength of the PSC coating. As described in previous studies,[29,30] the adhesion strength of the PSC coating was evaluated by ultrasonication tests. After oscillation in an ultrasonic wave (40 kHz) in PBS for 30 min, SEM (JOEL-6700, Japan) was performed to observe the changes in the PSC coating.

Bioactivity test of PSC-coated scaffolds. PSC-coated scaffolds were put into SBF at 1.5 mg mL^{-1} for 12 h. The surface morphologies were observed *via* SEM (JOEL-6700, Japan).

2.4 *In vitro* cell experiments

Cell culture. The rat BMSCs (Yi Fei Xue Biotech. Co., Nanjing, China) were chosen for *in vitro* experiments and cultured in the Dulbecco's Modified Eagle Medium/F-12 (DMEM/F-12, Gibco, Carlsbad, CA, USA) and osteogenic differentiation medium (Yi Fei Xue Biotech. Co., Nanjing, China). Cells were incubated at 37 °C in a humidified atmosphere of 5% CO_2.

Biocompatibility. The biocompatibilities of the two groups of scaffolds (Ti group and Ti-PSC group) were compared using Live–Dead staining assays. Scaffolds were laid on the bottom of the 48-well cell culture plates before the experiment. After disinfection under ultraviolet light for 30 min, BMSCs were seeded onto the scaffold in the 48-well cell culture plates at a density of 1×10^4 cells per well. They were stained with the live/dead staining solution composed of calcein-AM (2 μM) and propidium iodide (PI) (4 μM) after being incubated in the cell incubator for 24 h. The original culture medium was replaced by a live/dead staining solution for another incubation of 30 min in the dark. After being removed and washed with phosphate-buffered saline (PBS) three times, the scaffolds were observed under a confocal inverted laser microscope (C2-SIM, Nikon, Japan) at 10× magnification. The frequencies of excitation light were 488 nm and 561 nm.

Cell proliferation. The scaffolds (Ti group and Ti-PSC group) were placed on the bottom of 48-well cell culture plates. BMSCs were trypsinized in 0.25% pancreatic enzymes and suspended in DMEM/F-12. Cells were counted using a hemocytometer and an inverted light microscope (C2-SIM, Nikon, Japan). 100 μL of BMSC cell suspension was seeded in a 48-well plate at a density of 3×10^3 cells per well. Wells without scaffolds were used as the control group. At 1, 3, and 7 d of culture, 100 μL of Cell Counting Kit-8 (CCK-8) reagent was added to each well and the plate was further incubated at 37 °C for 2 h before the optical absorbance measurements at 450 nm wavelength. Five samples for each group were tested to obtain the mean value.

Cell adhesion. The scaffolds (Ti group and Ti-PSC group) were placed on the bottom of the 48-well cell culture plates. BMSCs were seeded on the scaffolds in the 48-well cell culture plates with a density of 1×10^4 cells per well. After being cultured for 2 d, the cells were fixed using the 4% paraformaldehyde solution and dehydrated using the ethanol solution with a level-by-level increase in the concentration of 30–50–70–85–95–100%. Two consecutive dehydrations were run at each level of concentration, with 30 min of immersion. After complete dehydration, platinum plating was performed in a vacuum, and cell morphology was observed *via* SEM (JOEL-6700, Japan).

Alkaline phosphatase (ALP) staining and quantitative assays. The scaffolds (Ti group and Ti-PSC group) were placed on the bottom of the 48-well cell culture plates. BMSCs (1×10^4 cells per well) were seeded and cultured in a 48-well plate with an osteogenic differentiation medium for 14 d. The medium was changed every 2 d. Cells were incubated using the BCIP/NBT Alkaline Phosphatase Color Development Kit (C3206, Beyotime Biotech. Co., Shanghai, China) for 60 min, and excess dyes were removed. ALP activity of each group of cells was evaluated using an Alkaline Phosphatase Assay Kit (P0321M, Beyotime Biotech. Co., Shanghai, China) and calculated from optical density (OD, 405 nm) values. The total intracellular protein content of cells was evaluated using a BCA Protein Assay Kit (P0011, Beyotime Biotech. Co., Shanghai, China) and calculated from optical density (OD, 560 nm) values. Six samples for each group were tested to obtain the mean value.

Alizarin red staining and semi-quantitative assay. The scaffolds (Ti group and Ti-PSC group) were placed on the bottom of the 48-well cell culture plates. BMSCs (1×10^4 cells per well) were seeded and cultured in a 48-well plate with an osteogenic differentiation medium for 28 d. Staining using the Alizarin Red S solution (G1452, Solarbio Biotech. Co., Beijing, China) was conducted to evaluate the mineralization. Cells were incubated with Alizarin Red S solution for 60 min, and excess dyes were removed. After image acquisition, the staining was performed using 100 mM cetylpyridinium chloride (Sigma-Aldrich, St. Louis, MO, USA) and the absorbance of the extract liquor was determined *via* spectrophotometry at 570 nm for semi-quantification.

2.5 Animal experiments

This animal experimental protocol was approved by the Laboratory Animal Welfare Ethics Branch of Peking University Institutional Review Board of Peking University Biomedical Ethics Committee (Approval Number: LA2021036).

Animal surgery. 24 adult male New Zealand white rabbits (weight 2.5 ± 0.2 kg) were randomly divided into a 3D-printed Ti6Al4V porous scaffold group without PSC coating (Ti group) and a PSC-coated 3D-printed Ti6Al4V porous scaffold group (Ti-PSC group), with 12 rabbits in each group.[29] General anesthesia of rabbits was performed using 3% isoflurane. As described in previous studies,[31] bilateral medial femoral condyles were prepared, disinfected, and exposed. An electric drill was used to drill a hole with a diameter of 5 mm and a depth of 6 mm on the medial condyle, and scaffolds of the Ti or Ti-PSC

groups were implanted, and the wound was closed layer by layer (ESI† Fig. S2). 4 00 000 units of penicillin were injected intramuscularly per day for the first 3 d after surgery to prevent infection.

At 4 weeks postoperatively, 6 rabbits were randomly selected in the Ti and Ti-PSC groups. After being euthanized with excessive CO_2, the distal femur specimens on the bilateral sides of each rabbit were taken out, with a total of 12 specimens in each group. Micro-computed tomography (micro-CT) analysis was performed on all 12 specimens, followed by 6 specimens randomly selected for bone histological analysis and the other 6 specimens for push-out tests. At 8 weeks postoperatively, the remaining 6 rabbits in each group were euthanized, and a similar experimental protocol was conducted.

Micro-CT. Micro-CT analysis was performed to analyze osteogenesis, bone ingrowth and osseointegration of specimens of the Ti and Ti-PSC groups. Scanning was performed using micro-CT (Siemens, Munich, Germany) with an X-ray source of 80 kV and a beam current of 80 mA. The scanning speed was 6° min^{-1} and the resolution was 9 μm. 3D visualization software (Inveon Research Workplace, Siemens, Munich, Germany) was used to analyze the data reconstructed by micro-CT. Metal scaffolds, bone tissues, and soft tissues were distinguished by CT values, where the CT values of the metal scaffolds, bone tissues, and soft tissues were >2250 Hounsfield units (HU), 1000–2250 HU, and <1000 HU, respectively. Regions of interest (ROIs) for quantitative analysis included the intra-porous region in the scaffold (intra-porous region), the region peripheral 500 μm around the scaffold (peri-implant region), and the sum of the two ROIs (total region). The bone volume/total volume (BV/TV), which is the proportion of new bone tissue volume to total volume, in each ROI was calculated.

Bone histology. Bone histology was also performed to analyze osteogenesis, bone ingrowth and osseointegration of specimens of the Ti and Ti-PSC groups. Femoral specimens were fixed in 4% paraformaldehyde for 14 d, followed by dehydration in graded ethanol (40%, 75%, 95%, and 100% ethanol for 3 d each) under vacuum. These specimens were then immersed in 4% paraformaldehyde for 14 d and cured using a light-curing embedding instrument (EXAKT520, EXAKT Apparatebau, Norderstedt, Germany). Then, a precision cutting and grinding system (EXAKT Cutting & Grinding System, EXAKT Apparatebau, Norderstedt, Germany) was used to cut the specimen from the middle of the scaffold along a circular cross-section. Both the left and right half specimens were ground and polished to sections of 40–50 μm. Goldner trichrome stain kit (Solarbio Biotech. Co., Beijing, China) was used to stain each section (new bone tissues, osteoid tissues, and scaffolds were stained green, red/orange, and black, respectively). Then, the stained sections were scanned using the NanoZoomer Digital Pathology Scanner (NDP Scan C13220-01, Hamamatsu Photonics K.K., Hamamatsu, Japan) and analyzed with Image-Pro Plus software version 6.0 (Media Cybernetics, Inc., Rockville, MD, USA). The analyzed ROI was the sum of the intra-porous region in the scaffold and the peripheral 500 μm region around the scaffold. The bone ingrowth proportion, which is the proportion of new bone tissue to the area of all pores, was calculated. The coverage of new bone on the surface of the scaffold was also compared between the two groups and the bone-to-implant contact ratio (BICR) was calculated according to the previous studies.[31–33]

Push-out test. The push-out test was performed using a mechanical testing system (Landmark, MTS Inc., Eden Prairie, MN, USA) to measure the fixation strength of the scaffold and bone. As described in previous studies,[34] the bone tissue at the bottom and top of the scaffold was carefully removed, and the specimen was fixed perpendicular to the horizontal plane in a special holder using polymethyl methacrylate (ESI† Fig. S3). The axial force was loaded on the scaffold at a constant rate of 1.5 mm min^{-1}, and the axial force-displacement curve was recorded. The endpoint of the test was a sudden drop in axial force, which was recorded as the maximum push-out force.

2.6 Statistical analysis

Continuous variables consistent with normal distribution were described by mean ± standard deviation (SD), and comparisons between two groups were performed using an independent sample *t*-test. SPSS software version 25.0 (SPSS, Inc., Chicago, IL, USA) was used for statistical analysis, and *P* values <0.05 were considered statistically significant.

3. Results and discussion

3.1 Fast sol–gel process for PSC preparation

A magnified version of video was taken to illustrate this rapid sol–gel process (ESI† Video S1 and Video S2). As shown in the video, the flowable sol-precursor quickly gelled once combined with water (ESI† Video S1) or steam (ESI† Video S2). After calcination of the above-sol, PSC was obtained. Since the concentration and usage of the precursor for PSC coating was thinner and less, the moisture in the air was enough to make it gelled in a short time, so a fast sol–gel process for PSC coating preparation was developed. This was really faster than the previous method reported by C. Y. Cui *et al.*,[25] in which the gelling takes more than two weeks.

3.2 Characterization of the PSC and PSC coating

Mechanical properties of the two groups of scaffolds (Ti group and Ti-PSC group). As shown in Table 1, there was no difference in the elastic modulus, stiffness, yield strength, and compression strength between the two groups of scaffolds (Ti group and Ti-PSC group) ($P > 0.05$). Mechanical properties were important features of Ti6Al4V scaffolds, which represented the load bearing capacity. Therefore, it is very important

Table 1 Mechanical properties of the two groups of scaffolds

Parameters	Ti group	Ti-PSC group	*T* value	*P* value
Elastic modulus (MPa)	1160 ± 122	1303 ± 108	−1.751	0.131
Stiffness (N mm^{-1})	3799 ± 401	4265 ± 355	−1.745	0.132
Yield strength (N)	1090 ± 100	1132 ± 154	−0.465	0.658
Compression strength (N)	1364 ± 134	1327 ± 102	0.427	0.684

that the coating of scaffolds should not negatively affect these properties. Considering the fact that the pore size and strut size of 3D-printed porous Ti6Al4V scaffolds were in the range of hundreds of micrometers whereas the thickness of the PSC coating was merely several micrometers, PSC coating would not significantly change the mechanical properties except bioactivity. H. Yang *et al.*[35] also found that Mesoporous Bioactive Glass coating did not markedly change the compressive strength of the original 3D-printed porous Ti6Al4V scaffolds.

pH of PSC dissolutions. As illustrated in Fig. 1A, the pH value of PSC dissolutions only slightly increased from 7.4 to 7.6. This is similar to the finding of Cui *et al.*,[25] wherein they discovered that PSC maintained the relatively neutral pH better than classical BGs like 45S5. Considering the fact that the physiological pH in the human body is close to 7.4, the negative impact of acidity or strong alkalinity on osteogenesis has long been known, while weak alkalinity was found to be beneficial to osteogenesis.[36] The pH of 45S5 dissolutions can significantly increase to 8.84, which was harmful to cell survival and differentiation. High PO_4^{3-} content in PSC corresponds to a high buffering ability of pH. Therefore, PSC, with relatively neutral pH, could provide a microenvironment more suitable for the proliferation and differentiation of cells.

Bioactivity test of PSC. As shown in Fig. 1B, it was evident that after 12 h of immersion in SBF, a large number of needle-like aggregates appeared on the surface of PSC, covering almost the entire surface, which exhibited the characteristic morphology of HA.[37,38] The aggregates grew denser with prolonged immersion, which demonstrated the excellent bioactivity of PSC. HA formation was further demonstrated by XRD (Fig. 1C), which have characteristic peaks of HA (25.9°, 31.7°, 32.8°, 39.7°, 46.6°, 49.6°, 53.2°, and 64.1°; JCPDS: 09-0432). On the FTIR spectrum (Fig. 1D), double absorption peaks at 607 cm^{-1} and 567 cm^{-1} as well as an enhanced band at 960 cm^{-1} were observed. Moreover, the band was enhanced with a longer immersion time, which further proved the formation of HA, which was important evidence of the bioactivity of BG.

Surface characterization of scaffolds. As shown in Fig. 2A, many pin-shaped pores appeared on the scaffolds after the alkali treatment. PSC was successfully coated on 3D-printed porous Ti6Al4V scaffolds and scaffolds could be observed in the

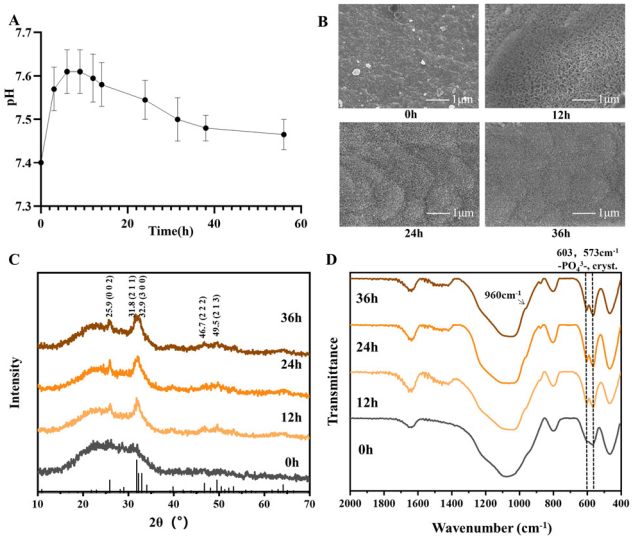

Fig. 1 pH and bioactivity test of PSC. (A) pH of PSC dissolutions. The pH value of PSC dissolutions only slightly increased from 7.4 to 7.6. (B) SEM of PSC in SBF for 0, 12, 24 and 36 h, respectively. Characteristic morphology of HA was found in 12 h and grew denser with prolonged immersion in 24 h and 36 h. (C) XRD of PSC in SBF for 0, 12, 24 and 36 h. Characteristic peaks of HA (25.9°, 31.7°, 32.8°, 39.7°, 46.6°, 49.6°, 53.2°, and 64.1°; JCPDS: 09-0432) were found. (D) FTIR of PSC in SBF for 0, 12, 24 and 36 h. Double absorption peaks at 607 cm^{-1} and 567 cm^{-1} as well as an enhanced band at 960 cm^{-1} were observed.

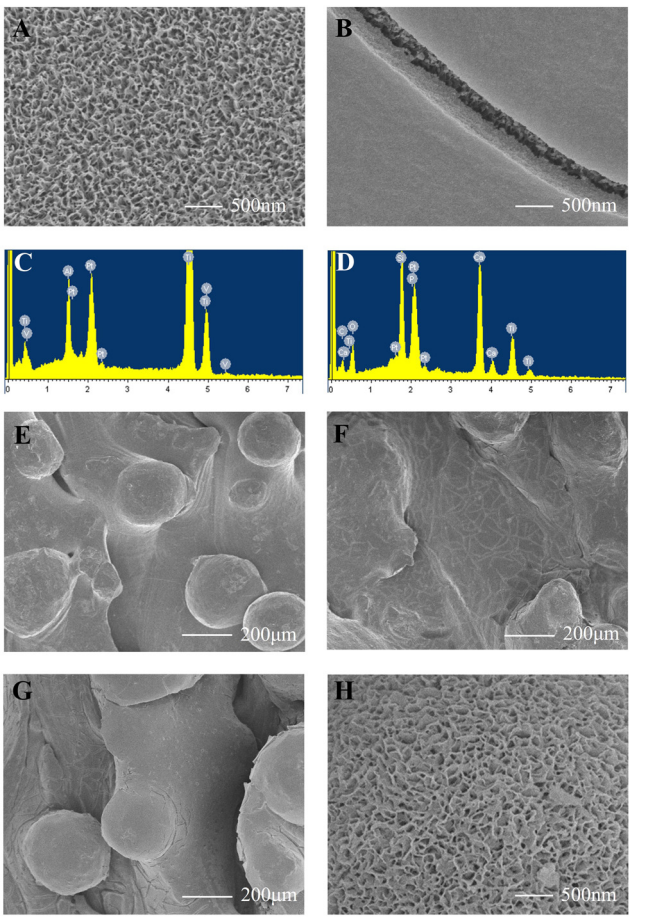

Fig. 2 Surface characterizations of scaffolds and adhesion strength of the PSC coating. (A) SEM of alkali-treated scaffolds. Many pin-shaped pores appeared on the scaffolds after the alkali treatment. (B) SEM of PSC-coated scaffolds. PSC was successfully coated on 3D-printed porous Ti6Al4V scaffolds and scaffolds could be observed in the cracks of the coating. (C) EDS of Ti6Al4V scaffolds. The main elements in Ti6Al4V scaffolds were Ti, Al, and V. (D) EDS of PSC-coated scaffolds. The main elements in the surface of PSC-coated scaffolds were Ti, Si, Ca, P, and O. (E) SEM of scaffolds of Ti6Al4V. Partially melted titanium alloy powder was seen. (F) SEM of PSC-coated scaffolds before ultrasonication tests. PSC coating was seen on the surface of the Ti6Al4V scaffold. (G) SEM of PSC-coated scaffolds after ultrasonication tests. No PSC-coating fragments were found to detach from the scaffold. (H) SEM of PSC-coated scaffolds in SBF for 12 h. Many needle-like aggregates appeared on the surface of PSC-coated scaffolds, a feature implying the likely formation of HA.

cracks of the coating (Fig. 2B). As shown in Fig. 2C and D, EDS demonstrated that the main elements in Ti group scaffolds were Ti, Al, and V, in agreement with its component (Ti6Al4V). The main elements in the surface of the Ti-PSC group scaffolds became Ti, Si, Ca, P, and O, reflecting the main component of PSC (P_2O_5, CaO, and SiO_2), proving the effective preparation of the coating.

Adhesion strength of the PSC coating. As shown in Fig. 2E–G, after oscillating in an ultrasonic wave (40 kHz) in PBS for 30 min, no PSC coating fragments were found to detach from the scaffold in SEM, indicating that this PSC coating is strongly bonded to the substrate.

Bioactivity test of PSC-coated scaffolds. After 12 h of immersion in SBF, many needle-like aggregates appeared on the surface of PSC-coated scaffolds (Fig. 2H), a feature implying the likely formation of HA.[37,38] HA formation was important evidence of the bioactivity, and the HA layer was also essential for the rapid bonding of bone and scaffolds. The rate of ion release was largely dependent on the specific surface area and the surface area of PSC was 45 times greater than that of 45S5. Consequently, more Si and P ions were released by PSC than by 45S5,which could contribute to the effective formation of HA.[25]

3.2 *In vitro* cell experiments

Biocompatibility. From the Live–Dead staining shown in Fig. 3A, it could be observed that the green fluorescence in the Ti-PSC group showed higher intensity and coverage, which proved that the cells in the Ti-PSC group were larger in number and more extended in morphology with longer pseudopodium, indicating better cell adhesion. Besides, the Ti group had a small amount of red fluorescence, while the Ti-PSC group had hardly any red fluorescence, which also proved the improvement of biocompatibility by PSC coating.

Cell proliferation. As shown in Fig. 3B, the cells in the Ti-PSC group were more viable than those in the Ti group at any interval. As PSC slowly dissolved into the culture medium, a significant difference ($P < 0.05$) occurred on Day 7, which means that PSC coating is beneficial for cell proliferation.

Cell adhesion. As displayed in Fig. 3C, cell morphologies of BMSCs 48 h after the seedings of the Ti group and Ti-PSC group, respectively, and the BMSCs were pointed by white arrow points. From this figure, it can be seen that BMSCs in the Ti group had fewer pseudopodia. BMSCs in the Ti-PSC group covered a larger area, and the pseudopodia showed a filament-like structure.

Quantitative tests were performed on the adhesion results. 15 cells within the SEM scope were randomly selected, and the number of pseudopodia and the length of the cells were recorded. The results are shown in Fig. 3D. Compared with the Ti group, BMSCs possessed twice as many pseudopodia (the number of pseudopodia in the Ti group was 3.1 ± 0.6, while the number of pseudopodia in the Ti-PSC group was 6.3 ± 1.2. $P < 0.05$). Moreover, the cell length in the Ti group was 35.8 ± 11.8, while the cell length in the Ti-PSC group was 87.9 ± 16.1. BMSCs cells had a wider coverage in the Ti-PSC group (2.4 times that of the Ti group with $P < 0.05$), which means that PSC coating is beneficial for cell adhesion.

ALP staining and quantitative assay. As shown in Fig. 3E, compared with the Ti group, there were more grey-black precipitates on the surface of the Ti-PSC group scaffolds. The two groups of ALP were 0.039 ± 0.007 (μmol min^{-1} mg^{-1} protein) and 0.077 ± 0.004 (μmol min^{-1} mg^{-1} protein) ($P < 0.05$), respectively, which confirms that PSC coating promotes BMSCs cell differentiations.

Alizarin red staining and semi-quantitative assay. As illustrated in Fig. 3F, compared with the Ti group, there were more dark red calcium nodules on the surface of Ti-PSC group scaffolds, which suggests a higher level of mineralization of cells. Absorbance was measured at 570 nm to semi-quantitatively assess the mineralization of BMSCs. The optical density (OD) values of the Ti and Ti-PSC groups were 0.336 ± 0.032 and 0.898 ± 0.083 ($P < 0.05$), respectively. The above observations demonstrate the promoting effects of PSC coating upon cell differentiation and mineralization at the early stages of BMSCs.

To summarize, the PSC-coated Ti6Al4V scaffolds showed superior biocompatibility, cell proliferation promotion, cell adhesion, osteogenic differentiation and mineralization compared to their bare counterparts *in vitro* cell experiments. Considering the fact that acidity or strong alkalinity was harmful to osteogenesis and high Si and P concentrations in the appropriate range were beneficial to cell proliferation and differentiation, PSC, with a relatively neutral pH and higher Si and P concentrations, could promote the biocompatibility, proliferation, adhesion, osteogenic differentiation and mineralization of BMSCs.[25,26]

3.3 Animal surgery

All surgical procedures on 24 rabbits were performed successfully, and no complications such as death and wound infection occurred within 8 weeks after surgery. All the scaffolds were in the original position, and there was no obvious infection or heterotopic ossification at the operative site when the distal femur specimens were taken out.

Micro-CT. As shown in Fig. 4A–K and Table 2, micro-CT showed that the total BV/TV and intra-porous BV/TV of the Ti-PSC group were higher than those of the Ti group at 4 and 8 weeks ($P < 0.05$). Meanwhile, the peri-implant BV/TV of the Ti-PSC group at 8 weeks was higher than that of the Ti group ($P < 0.05$), while although the average value of the peri-implant BV/TV at 4 weeks was also higher than that of the Ti group, the difference was not statistically significant ($P > 0.05$). This indicated that the new bone formation of the Ti-PSC group was more than that of the Ti group at 4 and 8 weeks, suggesting that PSC coating could promote the osteogenesis and bone ingrowth of 3D-printed Ti6Al4V porous scaffolds. Our previous studies also showed that PSC was pH-neutral, providing a favorable micro-environment for cell survival. PSC can also release higher content of silicate ions and phosphate ions, which can promote the proliferation, differentiation, mineralization, and osteogenesis of BMSCs. In animal experiments, PSC also significantly promoted the formation of new bone in the

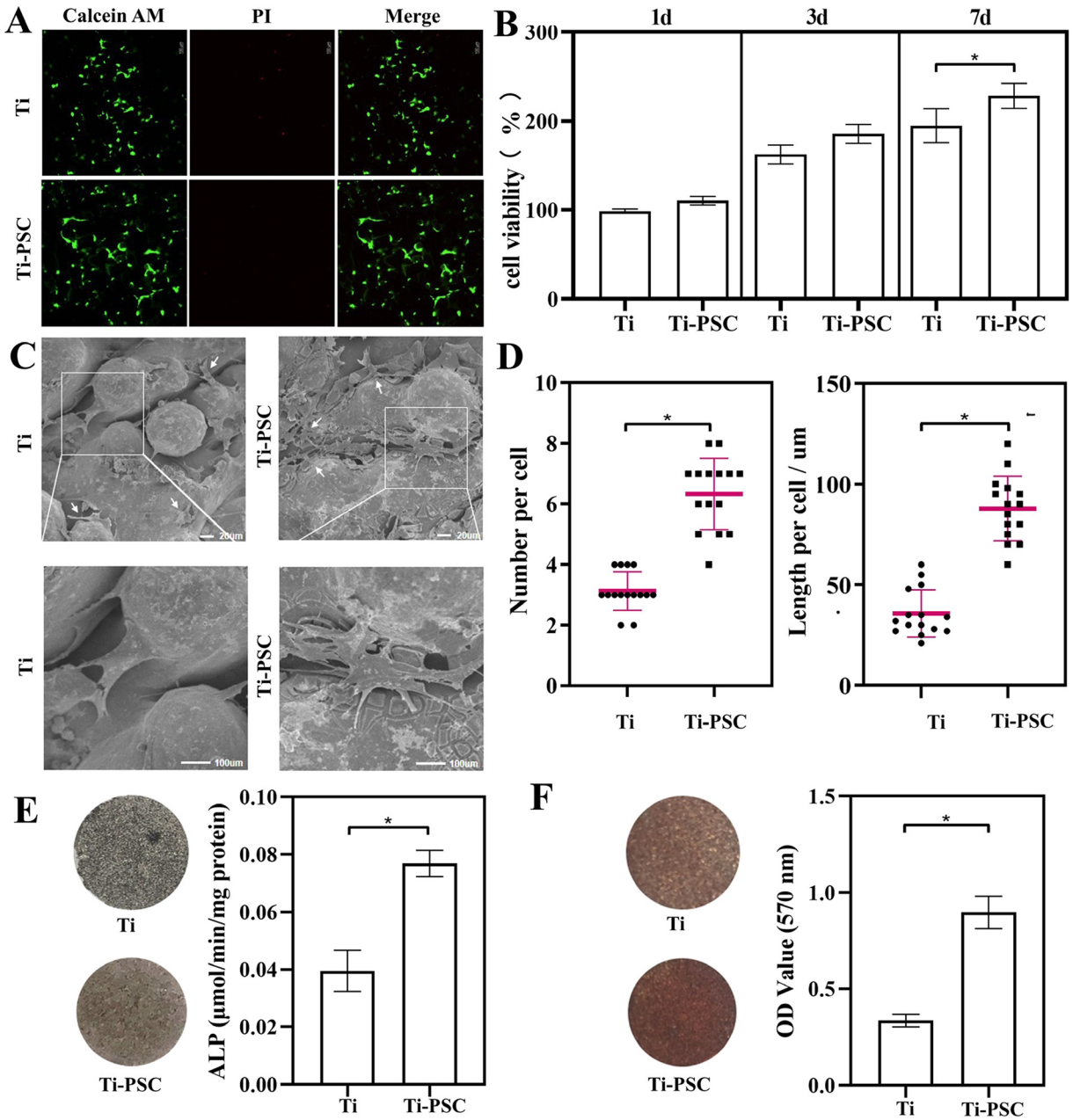

Fig. 3 Biocompatibility, cell proliferation, cell adhesion, cell differentiation and cell mineralization on two groups of scaffolds. (A) Live/dead staining of the scaffolds after 24 h of cell culture. Calcein-AM stained live cells and propidium iodide (PI)-stained dead cells. The intensity and coverage of green fluorescence were higher, and red fluorescence was less in the Ti-PSC group. (B) Cell proliferation on two groups of scaffolds. The cells in the Ti-PSC group were more viable than those in the Ti group at any interval, especially a significant difference ($P < 0.05$) occurred on Day 7. (C) SEM of BMSCs on two groups of scaffolds for 48 h. BMSCs in the Ti-PSC group covered a larger area, and the pseudopodia showed a filament-like structure. (D) The number of pseudopodia and the length of BMSCs on two groups of scaffolds for 2 days. The number of pseudopodia and the length of BMSCs in the Ti-PSC group were higher than those of the Ti group ($P < 0.05$). (E) ALP staining and quantitative assay on two groups of scaffolds for 14 days. There were more grey-black precipitates on the surface of the Ti-PSC group scaffolds with a higher amount of ALP ($P < 0.05$). (F) Alizarin red staining and semi-quantitative assay on two groups of scaffolds for 28 days. There were more dark red calcium nodules on the surface of the Ti-PSC group scaffolds with a higher amount of alizarin red ($P < 0.05$).

repair of calvarial bone defects in rats,[28] in agreement with our current findings.

Bone histology. As shown in Fig. 5A–E, the bone ingrowth proportions of the Ti-PSC group were both higher than that of the Ti group at 4 and 8 weeks (4 weeks: 47.08% ± 7.85% *vs.* 31.84% ± 9.33%, $P < 0.05$; 8 weeks: 50.82% ± 6.40% *vs.* 42.10% ± 6.24%, $P < 0.05$), which suggests that PSC coating can promote osteogenesis and bone ingrowth of 3D-printed Ti6Al4V porous scaffolds. This result was consistent with our previous research results[28] and was also consistent with the above micro-CT results.

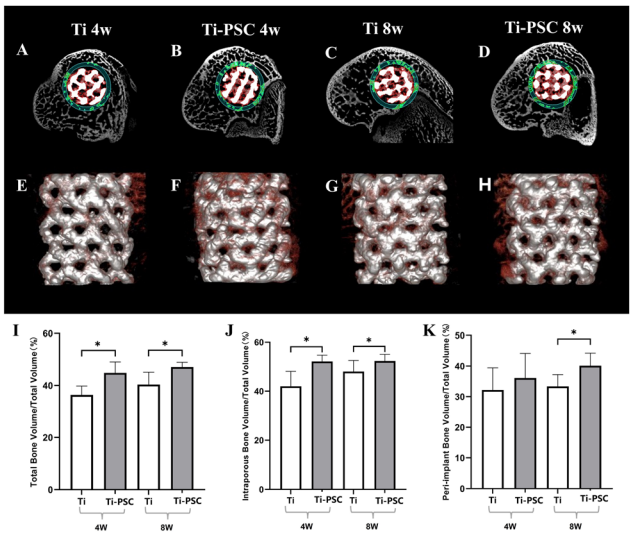

Fig. 4 Osteogenesis, bone in-growth, and osseointegration of Ti and Ti-PSC group scaffolds at 4 and 8 weeks in micro-CT. (A–D) Representative cross-sectional image of micro-CT (A: Ti group at 4 weeks; B: Ti-PSC group at 4 weeks; C: Ti group at 8 weeks; D: Ti-PSC group at 8 weeks). The scaffold was labelled in white. New bone in the intra-porous region was labelled in red and new bone in the peri-implant region was labelled in green. (E–H) Representative 3D-reconstructed images of micro-CT (E: Ti group at 4 weeks; F: Ti-PSC group at 4 weeks; G: Ti group at 8 weeks; H: Ti-PSC group at 8 weeks). The scaffold was labelled in silver and new bone was labelled in red. (I–K) Total (I), intra-porous (J), and peri-implant (K) Bone Volume/Total Volume of the Ti group scaffold and Ti-PSC group scaffold at 4 and 8 weeks in Micro CT. *: $P < 0.05$.

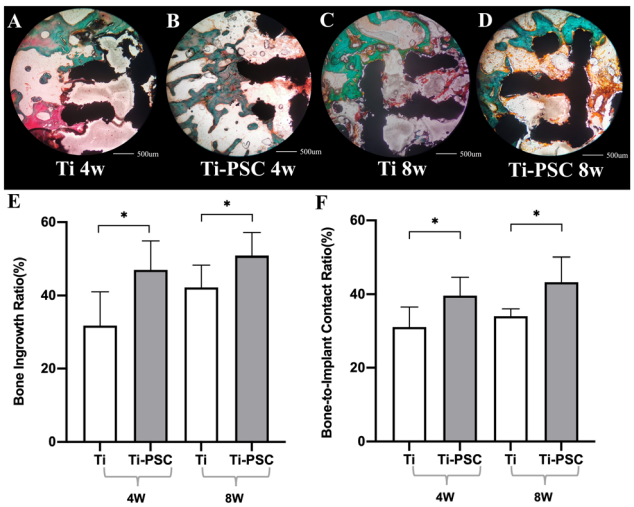

Fig. 5 Osteogenesis, bone in-growth, and osseointegration of Ti group scaffolds and Ti-PSC group scaffolds at 4 and 8 weeks in bone histology. (A–D) Representative images of bone histology: (A: Ti group at 4 weeks; B: Ti-PSC group at 4 weeks; C: Ti group at 8 weeks; D: Ti-PSC group at 8 weeks): The scaffold was stained black, new bone was stained green, and osteoid tissues were stained red or orange. (E) Bone ingrowth proportion of Ti group scaffolds and Ti-PSC group scaffolds at 4 and 8 weeks in bone histology. (F) Bone-to-implant contact ratio (BICR) of Ti group scaffolds and Ti-PSC group scaffolds at 4 and 8 weeks in bone histology. *: $P < 0.05$.

Meanwhile, we also found that BICR of the Ti-PSC group was higher than that of the Ti group at 4 and 8 weeks (4 weeks: 39.55% ± 4.96% *vs.*31.15% ± 5.40%, $P < 0.05$; 8 weeks: 43.32% ± 6.93% *vs.* 33.98% ± 2.13%, $P < 0.05$), indicating that the Ti-PSC group had better osteointegration. Our previous study also found that in the repair of calvarial bone defects in rats, the new bone tissues with lamellar bone morphology in the PSC group were more organized and continuous, suggesting that the PSC does not simply promote osteogenesis, more importantly, this osteogenesis is not disordered, *i.e.*, the PSC can indeed promote bone remodeling and osseointegration.[28]

Push-out test. As illustrated in Fig. 6A, the maximum push-out force results from the Ti and Ti-PSC groups at 4 weeks and 8 weeks. The maximum push-out force of the Ti-PSC group at 4 weeks was slightly higher than that of the Ti group, although the difference was not statistically significant (482.27N ± 27.42N *vs.* 435.96N ± 29.60N, $P > 0.05$), and the maximum push-out force of the Ti-PSC group at 8 weeks was significantly higher than that of the Ti group (555.69N ± 25.69N *vs.* 485.36N ± 22.28N, $P < 0.05$).

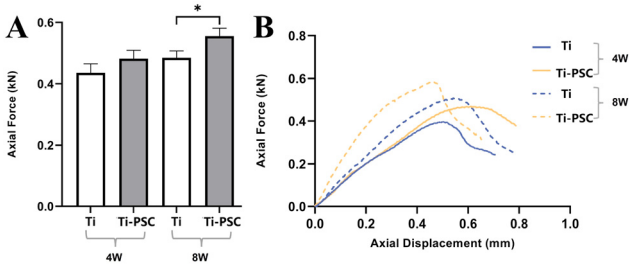

Fig. 6 Fixation strength of Ti and Ti-PSC group scaffolds at 4 and 8 weeks in the push-out test. (A) Maximum push-out force of the Ti group scaffold and Ti-PSC group scaffold at 4 and 8 weeks in the push-out test. *: $P < 0.05$.(B) Representative axial force-displacement curves of the Ti group scaffold and Ti-PSC group scaffold at 4 and 8 weeks in the push-out test.

Table 2 BV/TV of the Ti group and Ti-PSC group at 4 and 8 weeks

	4 w		8 w	
Parameters	Ti group (%)	Ti-PSC group (%)	Ti group (%)	Ti-PSC group (%)
Total BV/TV	36.29 ± 3.33	44.69 ± 4.02[a]	40.34 ± 4.71	47.20 ± 1.80[a]
Intra-porous BV/TV	42.16 ± 6.20	52.10 ± 2.44[a]	47.89 ± 4.58	52.31 ± 2.71[a]
Peri-implant BV/TV	32.09 ± 7.06	36.20 ± 8.04	33.35 ± 4.10	40.18 ± 4.08[a]

[a] At the same time, $P < 0.05$ when compared with Ti and Ti-PSC groups.

In Fig. 6B, the representative axial force-displacement curves of the two groups at 4 and 8 weeks are shown. The axial force-displacement curve of the Ti-PSC group was steeper than that of the Ti group at 4 weeks and 8 weeks, that is, to produce the same axial displacement of implant, the needed axial force of the Ti-PSC group was greater. This also indicates that the scaffolds of the Ti-PSC group had greater fixation strength of scaffold and bone, which was a compositive index of osteogenesis, bone in-growth, and osseointegration, and was also an objective expression of the implant stability.[39,40] Therefore, the PSC-coated 3D-printed Ti6Al4V porous implant is expected to improve the stability of the implant in clinical practice and has a good prospect for clinical application.

4. Conclusions

In this study, a pH neutral bioactive glass (PSC) was successfully coated on 3D-printed porous Ti6Al4V scaffolds with good adhesion strength. This *in situ* sol–gel method for fabricating PSC coating was simple, quick, and convenient. PSC-coated Ti6Al4V scaffolds showed superior biocompatibility, cell proliferation promotion, cell adhesion, osteogenic differentiation and mineralization compared to their bare counterparts *in vitro* and had more bone ingrowth and osseointegration as well as higher push-out strength of the implant *in vivo*. PSC coating is expected to improve the stability of the 3D-printed porous Ti6Al4V implants, which may be developed for immediate clinical applications.

Author contributions

Xinguang Wang: conceptualization, methodology, software, validation, formal analysis, investigation, writing – original draft, and visualization; Qirui Guo: methodology, software, validation, formal analysis, investigation, and writing – original draft; Yizhen He: methodology, software, validation, formal analysis, investigation, and writing – original draft; Xiao Geng: methodology, validation, formal analysis, investigation, and data curation; Cheng Wang: methodology, validation, formal analysis, and investigation; Yang Li: methodology, formal analysis, and investigation; Zijian Li: formal analysis and investigation; Caimei Wang: formal analysis, investigation, and writing – review & editing; Dong Qiu: conceptualization, formal analysis, investigation, data curation, writing – review & editing, supervision, project administration, and funding acquisition. Hua Tian: conceptualization, formal analysis, investigation, data curation, writing – review & editing, supervision, project administration, and funding acquisition.

Conflicts of interest

All authors have read the declaration of interests and declare that they have no competing interests.

Acknowledgements

This work was supported by the Natural Science Foundation of Beijing Municipality (grant number: 19L2160). The authors acknowledge the research support from the Department of Laboratory Animal Science of Peking University Health Science Center in the animal experiment and the Beijing AKEC Medical Co., Ltd in the manufacture of 3D-printed Ti6Al4V porous scaffolds.

Notes and references

1 H. H. Malik, A. R. Darwood, S. Shaunak, P. Kulatilake, A. A. El-Hilly, O. Mulki and A. Baskaradas, *J. Surg. Res.*, 2015, **199**, 512–522.
2 C. Serrano, H. van den Brink, J. Pineau, P. Prognon and N. Martelli, *J. Cranio-Maxillofac. Surg.*, 2019, **47**, 1387–1397.
3 V. Karageorgiou and D. Kaplan, *Biomaterials*, 2005, **26**, 5474–5491.
4 J. Lv, Z. Jia, J. Li, Y. Wang, J. Yang, P. Xiu, K. Zhang, H. Cai and Z. Liu, *Adv. Eng. Mater.*, 2015, **17**, 1391–1398.
5 J. Parthasarathy, B. Starly, S. Raman and A. Christensen, *J. Mech. Behav. Biomed. Mater.*, 2010, **3**, 249–259.
6 J. Liu, N. B. Mohd Rafiq, L. M. Wong and S. Wang, *Front. Chem.*, 2021, **9**, 768007.
7 B. G. X. Zhang, D. E. Myers, G. G. Wallace, M. Brandt and P. F. M. Choong, *Int. J. Mol. Sci.*, 2014, **15**, 11878–11921.
8 Z. Jing, T. Zhang, P. Xiu, H. Cai, Q. Wei, D. Fan, X. Lin, C. Song and Z. Liu, *Biomed. Mater.*, 2020, **15**, 052003.
9 S. B. Goodman, Z. Yao, M. Keeney and F. Yang, *Biomaterials*, 2013, **34**, 3174–3183.
10 X. Sheng, A. Wang, Z. Wang, H. Liu, J. Wang and C. Li, *Front. Bioeng. Biotechnol.*, 2022, **10**, 850110.
11 J. Lv, P. Xiu, J. Tan, Z. Jia, H. Cai and Z. Liu, *Biomed. Mater.*, 2015, **10**, 035013.
12 Y. Zhao, L. Bai, Y. Zhang, R. Yao, Y. Sun, R. Hang, X. Chen, H. Wang, X. Yao, Y. Xiao and R. Hang, *Biomaterials*, 2022, **288**, 121684.
13 X. Li, K. Xu, Y. He, B. Tao, K. Li, C. Lin, J. Hu, J. Wu, Y. Wu, S. Liu, L. Peng, H. Wang and K. Cai, *Biomaterials*, 2022, **287**, 121683.
14 P. Xiu, Z. Jia, J. Lv, C. Yin, Y. Cheng, K. Zhang, C. Song, H. Leng, Y. Zheng, H. Cai and Z. Liu, *ACS Appl. Mater. Interfaces*, 2016, **8**, 17964–17975.
15 R. Ni, Z. Jing, C. Xiong, D. Meng, C. Wei and H. Cai, *Ann. Transl. Med.*, 2022, **10**, 710.
16 J. R. Jones, *Acta Biomater.*, 2013, **9**, 4457–4486.
17 B. Begines, C. Arevalo, C. Romero, Z. Hadzhieva, A. R. Boccaccini and Y. Torres, *ACS Appl. Mater. Interfaces*, 2022, **14**, 15008–15020.
18 J. C. Moses and B. B. Mandal, *ACS Appl. Mater. Interfaces*, 2022, **14**, 14961–14980.
19 A. A. El-Rashidy, J. A. Roether, L. Harhaus, U. Kneser and A. R. Boccaccini, *Acta Biomater.*, 2017, **62**, 1–28.
20 X. V. Bui, V. B. Nguyen, T. T. H. Le and Q. M. Do, *Glass Phys. Chem.*, 2013, **39**, 64–66.

21 S. Ali, I. Farooq and K. Iqbal, *Saudi Dent. J.*, 2014, **26**, 1–5.
22 F. Baino, S. Hamzehlou and S. Kargozar, *J. Funct. Biomater.*, 2018, **9**, 25.
23 B. Ilharreborde, E. Morel, F. Fitoussi, A. Presedo, P. Souchet, G.-F. Penneçot and K. Mazda, *J. Pediatr. Orthop.*, 2008, **28**, 347–351.
24 X. Ye, S. Leeflang, C. Wu, J. Chang, J. Zhou and Z. Huan, *Materials*, 2017, **10**, 1244.
25 C. Y. Cui, S. N. Wang, H. H. Ren, A. L. Li, D. Qiu, Y. H. Gan and Y. M. Dong, *RSC Adv.*, 2017, **7**, 22063–22070.
26 A. Li and D. Qiu, *J. Mater. Sci.: Mater. Med.*, 2011, **22**, 2685–2691.
27 A. L. Li, H. H. Ren, Y. Cui, C. Wang, X. J. Zhou, H. Lin and D. Qiu, *J. Non-Cryst. Solids*, 2017, **475**, 10–14.
28 H. Zhao, G. Liang, W. Liang, Q. Li, B. Huang, A. Li, D. Qiu and D. Jin, *Mater. Sci. Eng., C*, 2020, **116**, 111249.
29 P. Yu, F. Lu, W. Zhu, D. Wang, X. Zhu, G. Tan, X. Wang, Y. Zhang, L. Li and C. Ning, *Appl. Surf. Sci.*, 2014, **313**, 947–953.
30 J. Ryu, S. H. Ku, H. Lee and C. B. Park, *Adv. Funct. Mater.*, 2010, **20**, 2132–2139.
31 Z. Jing, R. Ni, J. Wang, X. Lin, D. Fan, Q. Wei, T. Zhang, Y. Zheng, H. Cai and Z. Liu, *Bioact. Mater.*, 2021, **6**, 4542–4557.
32 K. Maekawa, K. Shimono, M. Oshima, Y. Yoshida, B. Van Meerbeek, K. Suzuki and T. Kuboki, *J. Oral Rehabil.*, 2009, **36**, 362–367.
33 S.-H. Jun, B. M. W. Chang, H.-P. Weber and J.-J. Kwon, *Int. J. Oral Maxillofac. Implants*, 2010, **25**, 985–990.
34 P. Xiu, Z. Jia, J. Lv, C. Yin, Y. Cheng, K. Zhang, C. Song, H. Leng, Y. Zheng, H. Cai and Z. Liu, *ACS Appl. Mater. Interfaces*, 2016, **8**, 17964–17975.
35 H. Yang, Q. Zhu, H. Qi, X. Liu, M. Ma and Q. Chen, *Materials*, 2018, **11**, 1540.
36 T. R. Arnett, *J. Nutr.*, 2008, **138**, 415S–418S.
37 T. Kokubo and H. Takadama, *Biomaterials*, 2006, **27**, 2907–2915.
38 K. Pluta, A. Sobczak-Kupiec, O. Półtorak, D. Malina and B. Tyliszczak, *J. Biomed. Mater. Res., Part A*, 2018, **106**, 1941–1950.
39 H. Liu, W. Li, C. Liu, J. Tan, H. Wang, B. Hai, H. Cai, H. J. Leng, Z. J. Liu and C. L. Song, *Biofabrication*, 2016, **8**, 045012.
40 H. Spece, C. Basgul, C. E. Andrews, D. W. MacDonald, M. L. Taheri and S. M. Kurtz, *J. Biomed. Mater. Res., Part B*, 2021, **109**, 1436–1454.

